

Lawrence Berkeley National Laboratory

Recent Work

Title

Effects of the c-Si/a-SiO₂ interfacial atomic structure on its band alignment: an ab initio study.

Permalink

<https://escholarship.org/uc/item/3n7952fk>

Journal

Physical chemistry chemical physics : PCCP, 19(48)

ISSN

1463-9076

Authors

Zheng, Fan
Pham, Hieu H
Wang, Lin-Wang

Publication Date

2017-12-01

DOI

10.1039/c7cp05879a

Peer reviewed

1 **The effects of c-Si/a-SiO₂ interface atomic structure on its band alignment: an**
2 ***ab initio* study**

3 Fan Zheng,¹ Hieu H. Pham,¹ and Lin-Wang Wang¹

4 ¹*Joint Center for Artificial Photosynthesis and Materials Sciences Division,*
5 *Lawrence Berkeley National Laboratory, Berkeley, California 94720, USA.*

6 The crystalline-Si/amorphous-SiO₂ (c-Si/a-SiO₂) interface is an important system used
7 in many applications, ranging from transistor to solar cell. The transition region of the
8 c-Si/a-SiO₂ interface plays a critical role in determining the band alignment between this
9 two regions. However, the question of how this interface band offset would be affected by
10 the transition region thickness and its local atomic arrangement, has yet fully investigated.
11 Here, by controlling the parameters of the classical Monte-Carlo bond switching algorithm,
12 we have generated the atomic structures of the interfaces with various thickness, as well
13 as containing Si at different oxidation states. Hybrid functional method, as shown by our
14 calculations to reproduce the *GW* and experimental results for bulk Si and SiO₂, are used
15 to calculate the electronic structure of the heterojunction. This allows us to study the
16 correlation between the interface band characterization and its atomic structures. We find
17 that although the systems with different thickness show quite different atomic structure
18 near the transition region, the calculated band offset tends to be the same, unaffected by
19 the detail interfacial structure. It is shown that our band offset calculation agrees well with
20 the experimental measurements. This robustness of the interface electronic structure to its
21 interfacial atomic details could be another reason for the success of the c-Si/a-SiO₂ interface
22 in Si based electronics applications. Nevertheless, when the reactive force field is used to
23 generate the a-SiO₂ and the c-Si/a-SiO₂ interface, the band offset significantly deviates from
24 the experimental values by about 1 eV.

25

I. INTRODUCTION

26 Amorphous oxides are often used as insulating, protection or carrier stopping layers for many
 27 electronic and optoelectronic applications. In such applications, the electronic structure of the sys-
 28 tem, e.g., the band alignment between the oxides and the underlying crystal substrate, as well as
 29 possible interface electronic states, are of high interest. Although density functional theory (DFT)
 30 interface studies become quite common, and they are often complemented by high level methods
 31 (like *GW*) band gap corrections, it is still relatively rare to find theoretical amorphous-crystal
 32 interface studies. This does not mean the crystal/amorphous interface is not important, quite
 33 the contrary, such interfaces exist in majority of electronic applications. The main reason for the
 34 lack of theoretical study is the difficulty to construct the reliable atomic structure of the interface,
 35 and to test such structures against experiment once structure is constructed. Furthermore, unlike
 36 the crystal/crystal interface, the crystal/amorphous interface often requires large supercells, which
 37 makes the calculation much more expensive. However, with the advance in computer power and
 38 computational algorithm, we can now calculate systems consisted with a few hundred atoms, and
 39 use methods like the hybrid functional which has a potential to describe the electronic structure
 40 more accurately than the local or semilocal functionals such as local density approximation (LDA)
 41 or generalized gradient approximations (GGA). On the other hand, the new applications of the
 42 amorphous oxide insulating or protection layer, e.g., in solar cell or solar electric chemical cell, and
 43 the push for a more fundamental understanding of their carrier dynamics, raise renewed interest
 44 of these systems. In this work, we use c-Si/a-SiO₂ as an example to study such crystal/amorphous
 45 interface. In particular, we like to compare different interfacial atomic structures and their elec-
 46 tronic structure consequences. From such a comparative study, we can estimate both the reliability
 47 of the different procedures to construct the atomic structure, as well as the physical understanding
 48 of different interfaces.

49 c-Si/a-SiO₂ interface is ubiquitous in Si based electronic devices. It is one of the most well stud-
 50 ied crystal-amorphous interface due to its predominance in electronic applications¹⁻¹⁶. Besides in
 51 the CMOS technology it is also widely used in other applications. For example, in photoelectro-
 52 chemistry, the amorphous SiO₂ has been one of the most popular protection layers to protect the
 53 light absorber, such as Si from being corroded by the electrolyte or water¹⁷. Current engineering
 54 technique can tune the thickness of SiO₂ film to as small as 0.6 nm, in order to improve the the gate
 55 capacitance in the metal-oxide-semiconductor capacitor, or to enhance the hole tunneling trans-
 56 port in silicon photoanode¹⁸. With such thin SiO₂, the details of the interface with Si becomes

extremely important. Different synthesizing and oxidation procedures might produce different interfacial atomic structure. Understanding the influence of the interfacial atomic structure to the electronic structure of system is therefore of great significance. In late 1980's, there were a burst of theoretical studies for c-Si/a-SiO₂. These studies have yielded band offsets in agreement with the experiments. But most of those studies are based on relatively small supercell systems in particular for *ab initio* calculations. Often, only one atomic structure is used, and there was no systematic comparison for different atomic structures. Moreover, most previous theoretical studies are based on LDA/GGA, with estimated postprocessing corrections to the LDA/GGA band gap error. In the current work, we use different strategies to construct the crystal/amorphous interface, and compare different interfacial atomic structures. We also use hybrid functional (HSE) to directly calculate the whole system without the need for further postprocessing corrections.

It is well known from early studies, one predominant feature of the c-Si/a-SiO₂ interface is its relative abruptness in the interfacial layers, as shown in TEM images¹⁷. Nevertheless, the interface can extend beyond one monolayers, to two or three atomic monolayers.¹⁹⁻²² Even a more extensive transition layer larger than 10 Å has been identified using X-rays^{8,23}. Within the transition region, photoemission and photoelectron spectroscopies demonstrate the presence of the suboxide layer^{20,21,24}, comprised of Si with oxidation states as Si⁺¹, Si⁺² and Si⁺³. Further measurements show their ratio to be 1:2:3 or 1:2:1 depending on synthesizing conditions^{25,26}. Meanwhile, molecular dynamics (MD) using reactive force field^{5,27} and Monte-Carlo (MC)²⁸ simulations have also shown the existence of beyond 10 Å interfacial layer. Owing to their relatively small computational costs, different valence force fields have been used to study both bulk a-SiO₂ and its interface with Si^{29,30}. The band gap and band offset were mainly computed using LDA or GGA method. However, the LDA/GGA methods do not always show agreement with the experimentally measured band offset due to the well-known issue of the band-gap underestimation. As a result, further corrections such as *GW* and hybrid functional have been used to correct the LDA/GGA band gaps, showing good agreement with the experiments³¹⁻³³. But as far as we know, there were no systematic study of electronic structures of different interfacial atomic structures, in particular using electronic structure calculation methods (e.g., the hybrid exchange-correlation functional) without postprocessing corrections directly.

As illustrated in both experimental and theoretical work, the size of the transition regions spans a broad range. As a result, the thickness of the interface is non-negligible when compared to the thickness of the SiO₂ layer for the thin SiO₂ layer applications. Therefore, understanding the effect of the transition region to the electronic structure of the interface is of great interest. In this

90 study, via the bond switching (BS) MC simulations, the thickness of the transition region will be
 91 measured by the maximum number of Si atoms connected via continued Si–Si bonds starting from
 92 the fixed crystal Si region. The band offset is computed using the hybrid functional methods. A
 93 special technique is developed which allows the application of a regional mixing parameter to the
 94 hybrid functional, hence able to describe the band gaps of both Si and SiO₂ regions accurately. Our
 95 results show excellent agreement with the experimental band offset, and also reveal a robustness
 96 of the band offset to the detail interfacial atomic profile.

97 II. CALCULATION METHODS

98 A. Monte-Carlo simulation

99 The continuous random network, or say the BS MC simulation, has been demonstrated to be
 100 an effective way to generate the amorphous structures for covalent bonding materials.^{34–37} During
 101 the BS procedure, a pair of nearby bonds, (either Si–Si or Si–O type bonds) are selected. This
 102 pair of bonds: A–B, C–D, are switched into a new pair of bonds: A–C, B–D. By enforcing the new
 103 bond topology into valence force field (VFF), the switched atomic structure is fully relaxed. The
 104 total energy of the relaxed structure is compared with the previous step, and this new structure
 105 is accepted or rejected following the Metropolis MC scheme. Many sophisticated force fields such
 106 as Tersoff and its derivatives^{38–41}, Yasukawa⁴², and Stillinger-Weber⁴³ potentials were applied to
 107 the studies of the Si/SiO₂ interface. However, many of such force fields are designed to break the
 108 bond, which does not apply to the continuous random network scheme. VFF as the simplest one
 109 is capable of describing the structure well, and it is straightforward to implement it into the BS
 110 MC scheme. In our simulation, the following VFF⁴⁴ is used to relax the structure.

$$E_{\text{tot}} = \frac{1}{2} \sum_i k_b (d_i - d_0)^2 + \frac{1}{2} \sum_{i,j} k_\theta (c_{ij} - c_0)^2 + U_{\text{repulsion}} \quad (1)$$

111 where $k_{b,\text{Si-O}} = 27 \text{ eV/\AA}^2$, $k_{b,\text{Si-Si}} = 9.08 \text{ eV/\AA}^2$, $k_{\theta,\text{Si-O-Si}} = 0.75 \text{ eV}$, $k_{\theta,\text{O-Si-O}} = 4.32 \text{ eV}$,
 112 $k_{\theta,\text{Si-Si-Si}} = 3.58 \text{ eV}$, and $k_{\theta,\text{Si-Si-O}} = (k_{\theta,\text{Si-Si-Si}} k_{\theta,\text{O-Si-O}})^{\frac{1}{2}} \text{ eV}$, d_0 and c_0 are taken from the
 113 DFT relaxed Si and SiO₂. The last term $U_{\text{repulsion}} = \frac{1}{2} \sum_{\langle i,j \rangle} k_r (d_{ij} - d_{\text{neighbor}})^4$ when $d_{ij} <$
 114 d_{neighbor} is to avoid the overlap of two atoms which are not directly connected by a bond. k_r is
 115 set to be 1 eV/\AA^4 . d_{neighbor} is taken differently depending on the two neighboring atomic species
 116 ($d_{\text{neighbor},\text{Si-O}} = 3.2\text{\AA}$, $d_{\text{neighbor},\text{O-O}} = 2.58\text{\AA}$, $d_{\text{neighbor},\text{Si-Si}} = 3.84\text{\AA}$). This term turns out to

117 be important to obtain reasonable structure, in particular near the interface^{29,30,34}. By taking
 118 derivative of the total energy to the atomic position, the force can be derived. With the total
 119 energy and the force as the inputs, the conjugate-gradient minimization scheme is used to relax
 120 the structure. Since the MC is used to obtain the bond topology for the amorphous structure, the
 121 accuracy of the relaxation is not crucial, and we set the force threshold to be 0.3 eV/Å.

122 The middle three layers of Si and their bonds are fixed in order to maintain the crystalline
 123 structure of Si (Fig. 1). However, if all other Si atoms are allowed to participate in the bond
 124 switch, it is easy to form the Si–Si bonds extended to the SiO₂ regions. These Si–Si bonds cause
 125 suboxide layers with Si⁺¹, Si⁺², Si⁺³ oxidation states. In order to quantify the thickness of this
 126 suboxide layer, we count the maximum number (n) of Si atoms connected via the continued Si–Si
 127 bonds starting from the fixed Si atom layer (Fig. 1). In our BS MC procedure, we deliberately
 128 limit n to be 2, 3 and 4 (e.g., to make a $n = 3$ suboxide layer, if n is larger than 3 during MC,
 129 the bond switch will be rejected) to generate different interfacial thickness. This allows us to
 130 have a systematic procedure to produce and thoroughly study different transition layers at various
 131 thicknesses. Here, $n=2$ corresponds to the "abrupt" interface with only one layer of atoms for
 132 the transition region, which has two Si–O bonds and two Si–Si bonds. Such abrupt interface
 133 is interesting since that is the case for most c-Si/c-SiO₂ interface constructed in many theoretical
 134 studies. It is interesting to note that it is possible to have such interface in the c-Si/a-SiO₂ interface
 135 structure. During the MC simulation, following previous literatures, the first $N/2$ steps BS steps
 136 are all accepted to fully amorphize the crystal at the beginning. Then, the stimulated annealing
 137 from very high temperature (10000K) is used to cool the structure and reduce the local strain.
 138 During the temperature cooling, a new temperature is set as 70% of the previous temperature
 139 step, and a total of around 300 thousand BS MC steps are performed to reach the equilibrium.

140 B. Reactive force field MD

141 We have also used MD simulation and "melt-and-quench" technique to obtain the c-Si/a-SiO₂
 142 along [001] direction using reactive force field (ReaxFF)⁴⁵ approach. More specifically, the inter-
 143 atomic interactions between Si–Si, Si–O and O–O pairs are characterized using the ReaxFF, which
 144 has been shown to reproduce well the structural properties of crystalline SiO₂. During the molecu-
 145 lar dynamics simulation, the Si part is kept frozen and the SiO₂ part was firstly heated up to high
 146 temperature until the crystals completely lose their structural memory. This is then equilibrated
 147 for a short period at this temperature (for 5 ps at 3500 K), followed by slowly cooling to room

148 temperature over 100 ps, which allows the formation of the SiO₂ amorphous phase. The time step
 149 for the MD simulations is 0.5 fs and the canonical ensemble (NVT, constant volume and constant
 150 temperature) was used. Here we followed the same procedure as employed by Kovacevic *et al* in
 151 our MD simulation details.⁴⁶

152 C. Electronic structure calculation

153 The plane-wave package PWmat^{47,48} is used to relax the DFT atomic structure and compute
 154 the electronic properties, using GGA exchange-correlation functional⁴⁹. The PWmat produces
 155 essentially the same results as that of Quantum Espresso⁵⁰, but with efficient GPU accelerations.
 156 The norm-conserving pseudopotential is used with a wavefunction energy cutoff of 50 Ryd with
 157 single Γ k -point⁵¹. In order to obtain the band offset, the last few snapshots from the end of the
 158 MC simulation are fully relaxed using DFT until all the components of the forces are below 0.05
 159 eV/Å. The local density of states are then computed to reveal the layer-resolved band energies
 160 along the direction perpendicular to the interface in order to illustrate the band offset.

161 However, such band offset obtained from GGA suffers from the underestimation of the band
 162 gap. Hybrid functional which includes the exact exchange integral has been shown to improve both
 163 the band gaps of bulk materials as well as the band offsets of the heterostructures⁵². Furthermore,
 164 the amount of exact exchange represented by a mixing parameter α , is inversely proportional
 165 to the high frequency dielectric constant of the material (ϵ_∞)⁵³. Thus, in theory, the mixing
 166 parameter for small band gap Si and the large band gap SiO₂ should be different. Indeed, this
 167 is true in practice. In our PWmat calculation using the norm conserving pseudopotentials, we
 168 found that a mixing parameter of 0.15 is needed for crystal Si and 0.35 is needed for crystal
 169 SiO₂ in order to yield their perspective band gaps of 1.12 and 8.5 eV. To solve this problem, we
 170 have introduced an atomic specific mixing parameter. More specifically, an atom-weighted mask
 171 function $f(\mathbf{r}) = 1 + \sum_i a_i e^{-(\mathbf{r}-\mathbf{R}_i)^2/\sigma^2}$ is introduced with a_i being atomic specific parameter for atom
 172 i , and R_i is the atomic position. Then the exchange interaction in the total energy expression can
 173 be written as: $\sum_{i,j} 0.25 o(i) o(j) \int \int \psi_i(\mathbf{r}) \psi_j^*(\mathbf{r}) f(r) \frac{\text{erfc}(\omega(\mathbf{r}-\mathbf{r}')}{|\mathbf{r}-\mathbf{r}'|} f(r') \psi_i^*(\mathbf{r}') \psi_j(\mathbf{r}') d^3\mathbf{r} d^3\mathbf{r}'$, here $\psi_i(\mathbf{r})$
 174 are wave functions, and $o(i)$ is its occupation number. The prefactor 0.25 is the original mixing
 175 parameter in the HSE. The local part of the GGA exchange energy density will also be modified
 176 by a factor of $1 - 0.25 f(r)^2$. By setting a_i for each atom type, an effective local mixing parameters
 177 can be achieved. We have determined the a_i parameters by requiring the hybrid functional to
 178 reproduce the experimental crystal Si and bulk amorphous SiO₂ band gaps as $a_{\text{Si,Silicon}} = -0.1$,

179 $a_{\text{Si},\text{O};\text{SiO}_2} = 0.24$. As we will demonstrate below, by implementing this method, the appropriate
 180 band offset can be obtained through a self-consistent hybrid functional calculation, which should
 181 provide more reliable electronic structures and wave function localizations than postprocessing
 182 corrections. Here, all the HSE calculations are done with the PWmat code, which has a fast
 183 scheme to calculate the HSE. For our 513 atom supercell system, with 2592 electron and 50 Ryd
 184 energy cutoff, the self-consistent HSE calculation takes about 4 hours using eight GPUs.

185 III. RESULTS AND DISCUSSIONS

186 A. Structure of the interface

187 To validate the effectiveness of the VFF and the BS MC method, we test our procedure by
 188 first building the amorphous bulk SiO_2 with 243 atoms. Shown in Fig. 2 is the calculated radial
 189 distribution functions (RDF) for the systems prepared by BS MC and ReaxFF MD, compared
 190 with the experimental values⁵⁴. From this graph, we can see that the BS MC method reproduces
 191 not only the peaks for short-range radius but also the main peaks for distance larger than 5 Å,
 192 demonstrating its validity in describing the amorphous feature of SiO_2 . For ReaxFF MD, although
 193 it predicts the first peak (Si–O bond) correctly, it deviates significantly from the experimental
 194 measured second peak (O–O distance), which may be caused by the lack of accuracy for the O–Si–
 195 O angle description. This can be further shown in Fig. 2b where the O–Si–O angle distributions
 196 of BS MC and ReaxFF MD amorphized structures are compared. As expected, most of the angles
 197 from BS MC simulation are around 109.5° , corresponding to the tetragonal cage of Si and O.
 198 However, the angles of the structure from the ReaxFF MD sample a broad range from 87° to
 199 143° . In particular, the small angles around 90° correspond to a significantly underestimated value
 200 ($\sim 2.3\text{Å}$) for O–O distance in the RDF.

201 With this confidence, we continue to explore the c-Si/a- SiO_2 interface using the BS MC sim-
 202 ulation. The initial structure is constructed by stacking the crystalline SiO_2 on Si along [001]
 203 direction albeit with significant strain on the crystalline SiO_2 . Here, the supercell $3\times 3\times 2$ of the
 204 cubic Si is used for the Si part of the interface with a and b -axis fixed to be the lattice constant of
 205 the Si crystal. The length of the c axis of the supercell is determined based on the experimental
 206 density of amorphous SiO_2 ^{29,55}. This initial structure is fully relaxed to relief the local strain at the
 207 interface with its resulting configuration as our initial atomic structure of the BS MC algorithm.
 208 It is followed by the BS MC with the procedure to control the interface thickness described above.

209 The last few snapshots from the MC simulations are used for DFT relaxations, and the resulting
 210 structures with different thickness of the transition regions are obtained and shown in Fig. 1. For
 211 all the structures with different interface thickness n , the SiO₂ part has been fully amorphized.
 212 When $n=2$, there is only a single atomic layer in the transition region, which mainly contains Si⁺²
 213 atoms. As n increases to 3 and 4, we notice the continued Si–Si bonds spreading into the SiO₂
 214 part (Fig. 1), forming all the five oxidation states of Si. In the mean while the number of layers
 215 containing suboxide Si atoms increases from monolayer to several atomic layers, expanding the
 216 transition regions.

217 Such expansion of the transition region can be further indicated by the characterization of
 218 the suboxide Si with its oxidation state determined by the number of the bonded oxygen atoms.
 219 Shown in Fig. 3 is the distribution of the oxidation states of Si along [001] direction under different
 220 thickness n . While, Si only shows 0 and +4 oxidation states deep inside Si and SiO₂ regions,
 221 suboxide Si becomes dominant near the interface. For example, the $n = 2$ structure shows the
 222 thinnest transition region, which occupies only single atomic layer (around 3Å). As n increases
 223 to 3 and 4, the transition region spans more layers, extending up to 5Å and 8Å, respectively.
 224 Furthermore, the ratio of these suboxide Si can be counted. In the case of $n = 2$, the ratio of states
 225 +1, +2 and +3 is distributed as 0:1:0 across the transition region. For $n = 3$ and $n = 4$, this ratio
 226 turns out to be 1:1.08:0.84 and 1:0.74:0.66, respectively. We see that the thicker interface has a
 227 more variety of Si valence states. The reported experimental value of this ratio varies widely, e.g.
 228 1:2:3 in Ref.25, 1:2:1 in Ref.26 This might depend sensitively on the synthesis conditions or the
 229 experimental probing techniques. At this point, it is difficult to make a quantitative comparison
 230 with any specific experiments. We find that the valence states of Si is in roughly similar orders
 231 between +1, +2 and +3 states in $n=3$ and 4 interfaces. Thus these experimental interface might
 232 not be the abrupt interface as illustrated in $n=2$ case.

233 B. Electronic structure

234 The band gap of interface is controlled by the band gap of Si part, which is around 1.1 eV.
 235 Taking $n = 2$ structure as an example, shown in Fig. 4 is the local density of states (LDOS)
 236 summed for the Si crystal part (Si⁰), amorphous SiO₂ part (Si⁺⁴ and O) and the transition part
 237 (Si⁺²), calculated using the local parameterized HSE functional. As shown from the density of
 238 states, the states near the band gap are dominant by the Si atoms inside the Si layer, without any
 239 defect states in the band gap. To show this more clearly, we plot the wavefunction in real space for

240 the conduction band minimum (CBM) and valence band maximum (VBM) as illustrated in Fig. 4
 241 b and c. It clearly shows that the wavefunctions are well localized inside the crystal Si. As for
 242 the Si^{+2} atoms in the transitional region, although they form only one atomic layer, their energies
 243 spread broadly for both low energy near the band gap (Si-like) and high energy away from the
 244 band gap (SiO_2 -like). This may be owing to their mutual bonds with Si and O atoms. However,
 245 the energies of the Si^{+4} atoms are pushed far away from the band gap by Si–O bonding, featuring
 246 the SiO_2 -like band energies.

247 The calculated LDOS is also used to estimated the "local" electronic structure and the band
 248 offset of the c-Si/a- SiO_2 interface. This is performed by averaging over the LDOS of the atoms
 249 within a given distance range along the [001] direction. Fig. 5a illustrates the GGA computed
 250 energies of CBM and VBM along the [001] direction for the $n=2, 3$ and 4 structures. The valence
 251 and conduction band offset (VBO and CBO) can be computed from the energy difference between
 252 the SiO_2 and Si parts, i.e. $\text{VBO} = \text{Max} [\text{VBM}_{\text{Si}} - \text{VBM}_{\text{SiO}_2}]$ and $\text{CBO} = \text{Max} [\text{CBM}_{\text{SiO}_2} - \text{CBM}_{\text{Si}}]$.
 253 For all the structures with different n we calculated, the CBO are around 1.8 eV, and the VBO
 254 are 2.5 eV, consistent with the other theoretical work^{7,52}.

255 Our results in Fig. 5 is a bit counter intuitive. For the $n=2,3,4$ cases, the amount of fixed bulk
 256 Si regions are the same. Intuitively, one expects the band offset starts at the same place from the
 257 bulk Si edge, and the thicker interfacial layer case of $n = 4$ should have a wider band offset turn-on
 258 region, just as the Si oxidation profile shown in Fig. 3. However, Fig. 5 shows that the band edge
 259 transition areas for $n = 2,3,4$ have similar thickness (sharpness). Furthermore, the bulk Si like band
 260 edge has been pushed out for the $n = 4$ case from the structurally bulk Si region. As a result, the
 261 effective bulk SiO_2 region for the $n = 4$ case is much shorter, while the electronic transition areas
 262 measured from LDOS are the same for $n = 2,3,4$. This will have significant consequence for the
 263 insulating capability and tunneling transport for the $n = 4$ case, particularly when the SiO_2 layer
 264 is thin. The reason for the push out of the Si bulk state into the transition area is that, whenever
 265 there are Si–Si bond, linking directly from the bulk Si area, the CBM and VBM wave function
 266 will be extended to those Si atoms, even though these Si atoms are already partially oxides as
 267 they also form Si–O bonds. This can be directly visualized from the real space wavefunctions for
 268 the band edges. Shown in Fig. 5b and c are the wavefunction for CBM and VBM of the $n=3$
 269 and 4 structures. Together with the $n=2$ case (Fig. 4b), these Si atoms in the SiO_2 part though
 270 partially oxidized, still contribute to the band edge states. Also due to this contribution, as well
 271 as local strains caused by the thicker interface, the VBM and VBM wavefunction isosurfaces look
 272 more disordered in Fig. 5b and c even in the region of c-Si for $n=3,4$, compared to the case of $n=2$

273 shown in Fig. 4b and c.

274 The second significant finding of our simulation is that the magnitudes of the band offsets are
 275 independent of the interfacial transition layer thickness. As shown from this graph (Fig. 5), the
 276 thickness of the transition region does not affect the value of the band offset significantly. Different
 277 n , although show quite different "local" band gaps near the transition region, the overall band
 278 offset is still determined by the states inside the Si and SiO₂ parts, unrelated to the details of the
 279 transition region. This means the band offset is not driven by an interfacial dipole moment, since
 280 such dipole moment should depend on the details of the transition layer. Instead, the intrinsic band
 281 positions of bulk Si and SiO₂ determine the band alignment. It is possible the random nature of
 282 the amorphous structure allows the system to avoid the large interfacial dipole moment. It remains
 283 to be seen if this is generally true to crystal/amorphous band alignment.

284 As mentioned above, the different mixing parameter α can be assigned to atoms locally. In order
 285 to obtain the appropriate α for Si and SiO₂, we evaluate the band gaps calculated by different α for
 286 crystalline Si and amorphous SiO₂ shown in Fig. 6 a and b, respectively. For the amorphous SiO₂,
 287 a 243-atom bulk structure ($3 \times 3 \times 3$ supercell) is used, generated by the same BS MC simulation
 288 procedure and relaxed by GGA, which is large enough to represent the SiO₂ part in the interface.
 289 From the linear relation of the band gap and a_i , the value of the a_i can be easily obtained to
 290 reproduce the experimental band gap. We choose $a_i = -0.1$ for Si at pure Si region, and 0.24 for Si
 291 and O in amorphous SiO₂ region. We employ this newly developed hybrid functional calculation
 292 method and compute the band offsets as shown in Fig. 6 c for the structures with $n=2, 3$ and 4.
 293 From this graph, the HSE-calculated band offsets display excellent agreement with the experiments,
 294 demonstrating the validity of the BS MC scheme and the newly developed HSE method. Besides the
 295 band offset, the HSE calculated results show similar features (e.g., the band edge wave functions)
 296 as the one calculated by the GGA method as discussed above. All the structures tend to have the
 297 unified band offset which is unrelated to the thickness of the transition regions. Similar to the GGA
 298 calculations, the bulk Si like band edge has been pushed into the SiO₂ region for the structures
 299 with "thick" transition regions (such as $n = 4$). Here, we want to emphasize that our HSE method
 300 does not need postprocessing corrections to the Si or SiO₂ separately, which provides a consistent
 301 description of the charge density, wavefunction and potential of the interface. These quantities can
 302 be used for further analysis such as charge transfer crossing the interface. We do note that, in the
 303 above, local density of state (LDOS) is used to determine the band offset. This could include the
 304 quantum confinement effect due to the small thickness of the c-Si layer. A common way to avoid
 305 such quantum confinement effect is to use local potential profile, instead of LDOS. However, the

LDOS determined band gap for the Si region is about 1.1 eV, similar to the result of the HSE bulk Si band gap. This indicates that the quantum confinement effect in this system is relatively small. This is probably because the Si effective masses of both the conduction band in the Γ -X direction, and the valence band heavy-hole, are rather large.

As aforementioned, we also calculate the band offset of the structure prepared by the ReaxFF MD simulation. By taking the snapshots out of the MD trajectory after equilibration, the electronic structure and band offset of the a-SiO₂/c-Si interface are calculated using GGA. The direct structure prepared by the MD simulated annealing usually do have one or two defect states due to imperfect bonding topology. However, a small amount of hydrogen atoms can be used to compensate the dangling bonds at those defect sites to eliminate the in-the-gap defect states. The band gap, CBO and VBO from GGA calculations are 0.76, 2.92 and 2.06 eV, respectively. It is also shown that both the CBM and VBM come from the Si part, which suggests a straddling type of band alignment similar to BS results (Fig. 5). As a summary, Table I summarizes the calculated band offsets from BS MC and ReaxFF MD simulations. Since the GGA calculated ReaxFF CBO is 1 eV higher than the results of BS MC, it indicates that that GGA band corrected band offset would be 1 eV off from that of the experimental results. Such deviation with the ReaxFF MD simulation may arise from the less accurate O-Si-O angle description as well as the dangling bonds emerging during the MD. Although ReaxFF allows ones to simulate the process of bond breaking and bond formation, which is quite relevant for the formation of amorphous structure in this case, the final structure would be subject to how the force fields were trained, typically against DFT-derived energies as well as the simulated annealing procedure. Nevertheless, if an accurate ReaxFF is obtained, and sufficient simulation time is possible, the ReaxFF can be used to simulate the actual synthesis process, which is missing in the BS MC method. In contrary, BS MC using VFF conserves the bonding orders to avoid the dangling bond. Thus by design, the BS MC gives better covalent bonding topology, leading to less defect. This however also lacks some real situations such as the bonding defects in reality. In practice, we found that the BS MC provides better amorphous structure in our calculation.

IV. CONCLUSION

Although the crystalline Si/amorphous SiO₂ is widely used for numerous applications, its band offset dependence on the thickness of the transitional region is not fully explored. In this work, by performing bond switching Monte-Carlo simulation and first-principle calculations, we have

TABLE I. Conduction and valence band offsets (eV) computed by ReaxFF MD, BS MC, and the HSE corrected BS. Other computational work with GGA or LDA and the experimental results are listed for comparison.

	ReaxFF	BS	BS-HSE	Other work (GGA/LDA)	Expt.
Conduction band offset	2.9	1.8	2.9	1.8 ⁷ , 2.3 ⁵²	3.0 ⁵⁶
Valence band offset	2.1	2.5	4.4	2.5 ⁷ , 2.5 ⁵²	4.3 ⁵⁷

337 studied the band offset of crystalline Si/amorphous SiO₂ interface under different thickness of
 338 the transitional region. For these structures with different thickness, we find that, although the
 339 detailed atomic structures near the interface differs significantly, the band offsets of all the different
 340 thickness tend to be the same. On the other hand, the bulk Si band edge feature has been extended
 341 into the transition area, which leads to a smaller effective SiO₂ region. Our calculation shows
 342 that the band offset is rather robust against the details of the transition layers. This is a major
 343 advantage for electronic devices, since it can reduce the device variations, a major issue when
 344 the device length shrinks to nano size. As a comparison, we also performed reactive force field
 345 molecular dynamics simulation to construct the interface. The calculated band offset shows that
 346 bond switching method tends to give more consistent results with the experiment, both for the
 347 atomic structure and electronic band offset. Moreover, by applying the newly developed hybrid
 348 functional with atomic specific mixing parameters, we can correct the band gap of Si and amorphous
 349 SiO₂ simultaneously in one heterostructure calculation, thus it can be used for future studies like
 350 transports and defect state carrier localizations.

351 V. ACKNOWLEDGMENT

352 This material is based on the work performed by the Joint Center for Artificial Photosynthesis,
 353 a DOE Energy Innovation Hub, supported through the Office of Science of the U.S. Depart-
 354 ment of Energy under Award number DE-SC0004993. We use the resource of National Energy
 355 Research Scientific Computing center (NERSC) located in Lawrence Berkeley National Laboratory.

356

357 ¹ S. C. Witczak, J. S. Suehle, and M. Gaitan, *Solid-State Electronics* **35**, 345 (1992).

- 358 ² A. C. Diebold, D. Venables, Y. Chabal, D. Muller, M. Weldon, and E. Garfunkel, *Materials Science in*
359 *Semiconductor Processing* **2**, 103 (1999).
- 360 ³ A. Stesmans and V. V. Afanas'ev, *Journal of Physics: Condensed Matter* **10**, L19 (1998).
- 361 ⁴ Z. H. Lu, M. J. Graham, D. T. Jiang, and K. H. Tan, *Applied Physics Letters* **63**, 2941 (1993).
- 362 ⁵ D. A. Muller, T. Sorsch, S. Moccio, F. H. Baumann, K. Evans-Lutterodt, and G. Timp, *Nature* **399**,
363 758 (1999).
- 364 ⁶ S. Dumpala, S. R. Broderick, U. Khalilov, E. C. Neyts, A. C. T. van Duin, J. Provine, R. T. Howe, and
365 K. Rajan, *Applied Physics Letters* **106**, 011602 (2015).
- 366 ⁷ F. Giustino, A. Bongiorno, and A. Pasquarello, *Journal of Physics: Condensed Matter* **17**, S2065 (2005).
- 367 ⁸ S. D. Kosowsky, P. S. Pershan, K. S. Krisch, J. Bevk, M. L. Green, D. Brasen, L. C. Feldman, and P. K.
368 Roy, *Applied Physics Letters* **70**, 3119 (1997).
- 369 ⁹ F. Giustino and A. Pasquarello, *Physical Review Letters* **95** (2005), 10.1103/PhysRevLett.95.187402.
- 370 ¹⁰ T. Watanabe, *Japanese Journal of Applied Physics* **38**, L366 (1999).
- 371 ¹¹ D. Fischer, A. Curioni, S. Billeter, and W. Andreoni, *Applied Physics Letters* **88**, 012101 (2006).
- 372 ¹² Z. Huiwen, L. Yongsong, M. Lingfeng, S. Jingqin, Z. Zhiyan, and T. Weihua, *Journal of Semiconductors*
373 **31**, 082003 (2010).
- 374 ¹³ A. Pasquarello, M. S. Hybertsen, and R. Car, *Physical Review Letters* **74**, 1024 (1995).
- 375 ¹⁴ A. Pasquarello, M. S. Hybertsen, and R. Car, *Physical Review B* **53**, 10942 (1996).
- 376 ¹⁵ T. Yamasaki, C. Kaneta, T. Uchiyama, T. Uda, and K. Terakura, *Physical Review B* **63** (2001),
377 10.1103/PhysRevB.63.115314.
- 378 ¹⁶ K. Kutsuki, T. Ono, and K. Hirose, *Science and Technology of Advanced Materials* **8**, 204 (2007).
- 379 ¹⁷ B. E. Deal and C. R. Helms, *The Physics and Chemistry of SiO₂ and the Si-SiO₂ Interface* (Springer
380 Science & Business Media, 2013) google-Books-ID: dg73BwAAQBAJ.
- 381 ¹⁸ P. F. Satterthwaite, A. G. Scheuermann, P. K. Hurley, C. E. D. Chidsey, and P. C. McIntyre, *ACS*
382 *Applied Materials & Interfaces* **8**, 13140 (2016).
- 383 ¹⁹ A. Bongiorno, A. Pasquarello, M. S. Hybertsen, and L. C. Feldman, *Physical Review Letters* **90** (2003),
384 10.1103/PhysRevLett.90.186101.
- 385 ²⁰ F. Rochet, C. Poncey, G. Dufour, H. Roulet, C. Guillot, and F. Sirotti, *Journal of Non-Crystalline Solids*
386 *Structure and Defects in SiO₂*, *Fundamentals and Applications*, **216**, 148 (1997).
- 387 ²¹ F. J. Himpsel, F. R. McFeely, A. Taleb-Ibrahimi, J. A. Yarmoff, and G. Hollinger, *Physical Review B*
388 **38**, 6084 (1988).
- 389 ²² K. Kimura and K. Nakajima, *Applied Surface Science Proceedings of the Fourth International Symposium*
390 *on the Control of Semiconductor Interfaces Karuizawa, Japan, October 21-25, 2002*, **216**, 283 (2003).
- 391 ²³ N. Awaji, *Japanese Journal of Applied Physics* **35**, L67 (1996).
- 392 ²⁴ T. Suwa, A. Teramoto, K. Nagata, A. Ogura, H. Nohira, T. Muro, T. Kinoshita, S. Sugawa, T. Ohmi,
393 and T. Hattori, *Microelectronic Engineering Insulating Films on Semiconductors 2013*, **109**, 197 (2013).

- 394 ²⁵ J. H. Oh, H. W. Yeom, Y. Hagimoto, K. Ono, M. Oshima, N. Hirashita, M. Nywa, A. Toriumi, and
395 A. Kakizaki, *Physical Review B* **63**, 205310 (2001).
- 396 ²⁶ G. Lucovsky and J. C. Phillips, *Journal of Physics: Condensed Matter* **16**, S5139 (2004).
- 397 ²⁷ A. C. T. Van Duin, A. Strachan, S. Stewman, Q. Zhang, X. Xu, and W. A. Goddard, *J. Phys. Chem.*
398 *A* **107**, 3803 (2003).
- 399 ²⁸ K.-O. Ng and D. Vanderbilt, *Physical Review B* **59**, 10132 (1999).
- 400 ²⁹ S. Lee, R. J. Bondi, and G. S. Hwang, *Journal of Applied Physics* **109**, 113519 (2011).
- 401 ³⁰ S. von Alfthan, A. Kuronen, and K. Kaski, *Physical Review B* **68** (2003), 10.1103/PhysRevB.68.073203.
- 402 ³¹ T. Anh Pham, T. Li, H.-V. Nguyen, S. Shankar, F. Gygi, and G. Galli, *Applied Physics Letters* **102**,
403 241603 (2013).
- 404 ³² A. Alkauskas, P. Broqvist, F. Devynck, and A. Pasquarello, *Phys. Rev. Lett.* **101**, 106802 1 (2008).
- 405 ³³ B. R. Tuttle, *Physical Review B* **70** (2004), 10.1103/PhysRevB.70.125322.
- 406 ³⁴ Y. Tu, J. Tersoff, G. Grinstein, and D. Vanderbilt, *Physical Review Letters* **81**, 4899 (1998).
- 407 ³⁵ H. H. Pham, G. T. Barkema, and L.-W. Wang, *Physical Chemistry Chemical Physics* **17**, 26270 (2015).
- 408 ³⁶ N. Mousseau and G. T. Barkema, *Journal of Physics: Condensed Matter* **16**, S5183 (2004).
- 409 ³⁷ L. Kong and L. J. Lewis, *Physical Review B* **77**, 085204 (2008).
- 410 ³⁸ J. Tersoff, *Physical Review B* **38**, 9902 (1988).
- 411 ³⁹ J. Tersoff, *Physical Review B* **39**, 5566 (1989).
- 412 ⁴⁰ S. R. Billeter, A. Curioni, D. Fischer, and W. Andreoni, *Physical Review B* **73**, 155329 (2006).
- 413 ⁴¹ J. Yu, S. B. Sinnott, and S. R. Phillpot, *Physical Review B* **75**, 085311 (2007).
- 414 ⁴² A. Yasukawa, *JSME international journal. Ser. A, Mechanics and material engineering* **39**, 313 (1996).
- 415 ⁴³ T. Watanabe, H. Fujiwara, H. Noguchi, T. Hoshino, and I. Ohdomari, *Japanese Journal of Applied*
416 *Physics* **38**, L366 (1999).
- 417 ⁴⁴ Y. Tu and J. Tersoff, *Physical Review Letters* **84**, 4393 (2000).
- 418 ⁴⁵ A. C. T. van Duin, A. Strachan, S. Stewman, Q. Zhang, X. Xu, and W. A. Goddard, *The Journal of*
419 *Physical Chemistry A* **107**, 3803 (2003).
- 420 ⁴⁶ G. Kovacevic and B. Pivac, *Journal of Applied Physics* **115**, 043531 (2014).
- 421 ⁴⁷ W. Jia, Z. Cao, L. Wang, J. Fu, X. Chi, W. Gao, and L.-W. Wang, *Computer Physics Communications*
422 **184**, 9 (2013).
- 423 ⁴⁸ W. Jia, J. Fu, Z. Cao, L. Wang, X. Chi, W. Gao, and L.-W. Wang, *Journal of Computational Physics*
424 **251**, 102 (2013).
- 425 ⁴⁹ J. P. Perdew, K. Burke, and M. Ernzerhof, *Phys. Rev. Lett.* **77**, 3865 (1996).
- 426 ⁵⁰ P. Giannozzi, S. Baroni, N. Bonini, M. Calandra, R. Car, C. Cavazzoni, D. Ceresoli, G. L. Chiarotti,
427 M. Cococcioni, I. Dabo, A. D. Corso, S. de Gironcoli, S. Fabris, G. Fratesi, R. Gebauer, U. Gerstmann,
428 C. Gougoussis, A. Kokalj, M. Lazzeri, L. Martin-Samos, N. Marzari, F. Mauri, R. Mazzarello, S. Paolini,
429 A. Pasquarello, L. Paulatto, C. Sbraccia, S. Scandolo, G. Sclauzero, A. P. Seitsonen, A. Smogunov,
430 P. Umari, and R. M. Wentzcovitch, *J. Phys.: Condens. Matter* **21**, 395502 (2009).

- 431 ⁵¹ D. R. Hamann, *Physical Review B* **88**, 085117 (2013).
- 432 ⁵² A. Alkauskas, P. Broqvist, F. Devynck, and A. Pasquarello, *Physical Review Letters* **101** (2008),
433 10.1103/PhysRevLett.101.106802.
- 434 ⁵³ J. H. Skone, M. Govoni, and G. Galli, *Physical Review B* **89** (2014), 10.1103/PhysRevB.89.195112.
- 435 ⁵⁴ S. Susman, K. J. Volin, D. L. Price, M. Grimsditch, J. P. Rino, R. K. Kalia, P. Vashishta, G. Gwanmesia,
436 Y. Wang, and R. C. Liebermann, *Physical Review B* **43**, 1194 (1991).
- 437 ⁵⁵ K. Laaziri, S. Kycia, S. Roorda, M. Chicoine, J. L. Robertson, J. Wang, and S. C. Moss, *Physical Review*
438 *B* **60**, 13520 (1999).
- 439 ⁵⁶ V. V. Afanas'ev, M. Houssa, A. Stesmans, and M. M. Heyns, *Applied Physics Letters* **78**, 3073 (2001).
- 440 ⁵⁷ J. W. Keister, J. E. Rowe, J. J. Kolodziej, H. Niimi, T. E. Madey, and G. Lucovsky, *Journal of Vacuum*
441 *Science & Technology B: Microelectronics and Nanometer Structures Processing, Measurement, and*
442 *Phenomena* **17**, 1831 (1999).

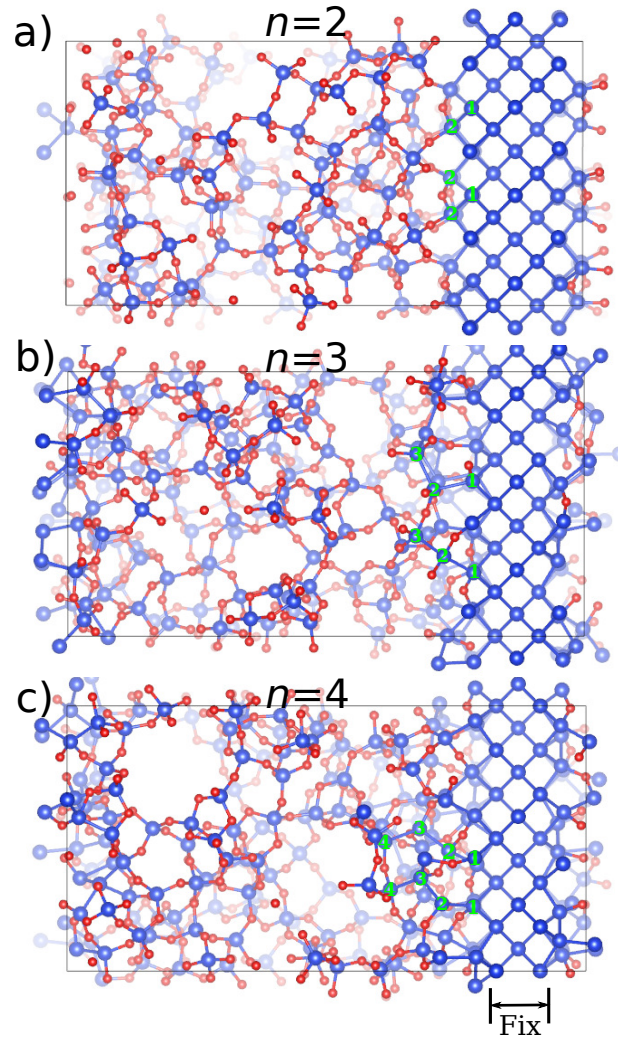


FIG. 1. The DFT relaxed structures taking from the MC simulations. Here, different maximum number of Si atoms (n) connected via the continued Si-Si bonds are used to represent the thickness of the transition region. a) $n = 2$, b) $n = 3$, and c) $n = 4$. The green digits are used to count the Si atoms which are connected by continued Si-Si bonds spreading from the fixed Si atoms as examples. The middle three Si layer are fixed in MC simulation and DFT relaxation. The Si-Si bonds connected to these fixed atoms are not allowed to switch during the MC simulation.

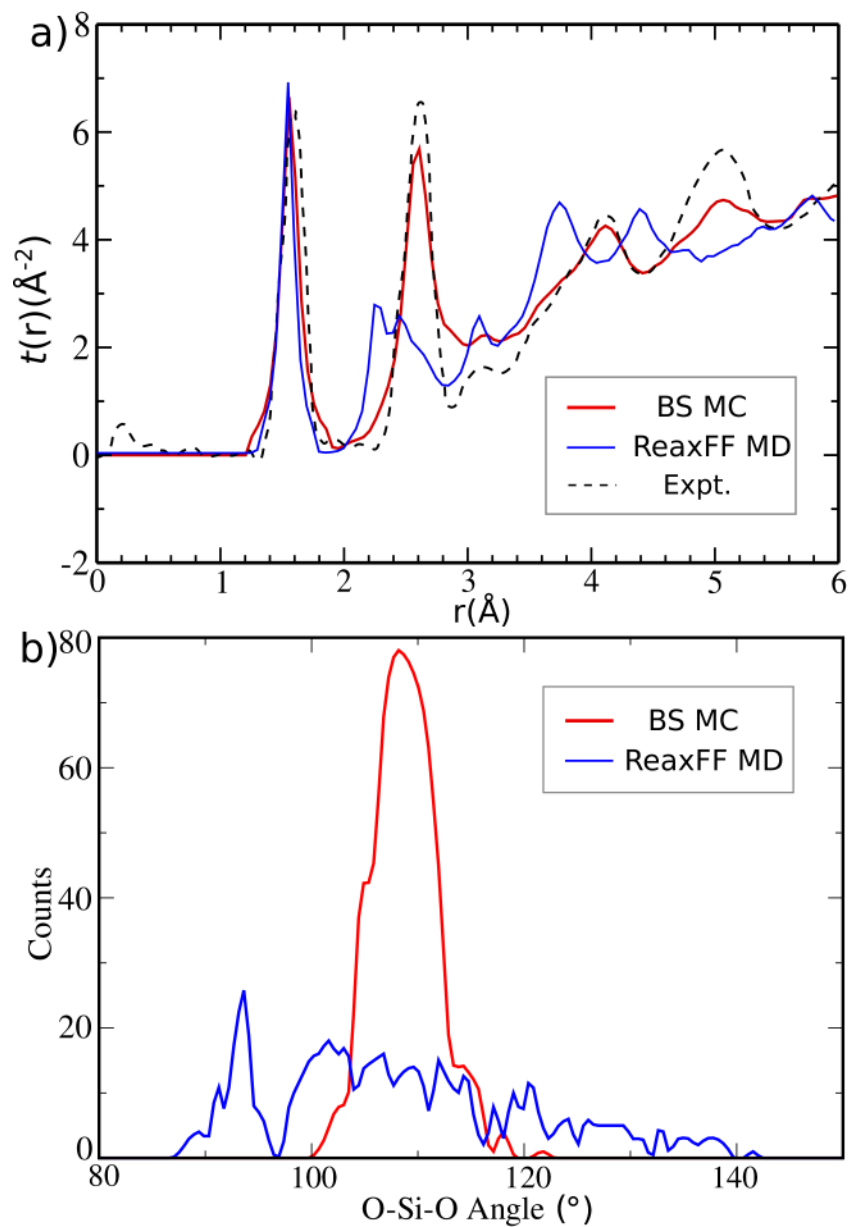


FIG. 2. a) Radial distribution function (RDF) comparison from BS MC, ReaxFF MD and experimental values. b) O-Si-O angle distribution histogram of the structures from BS MC and ReaxFF MD.

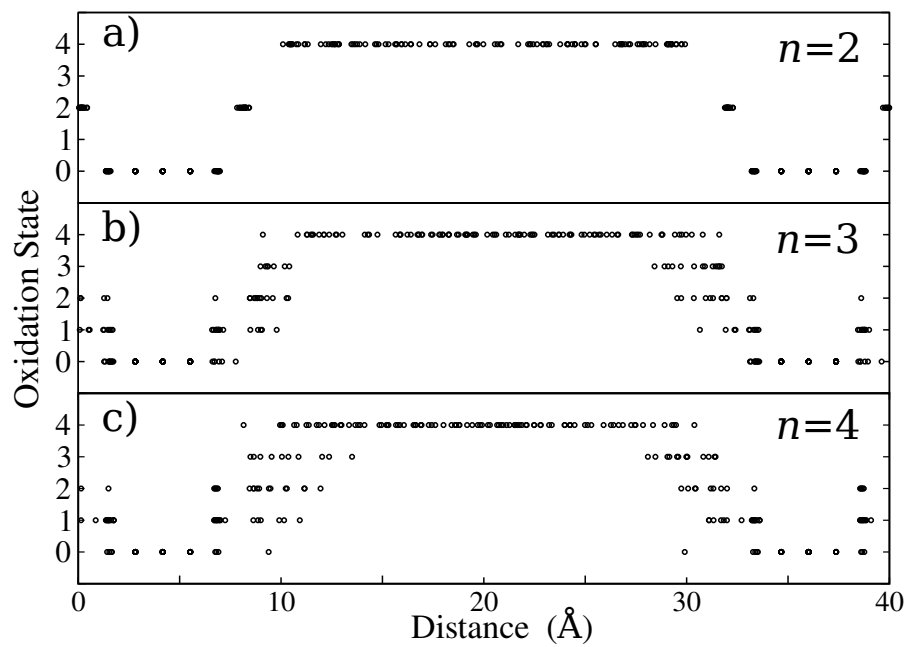


FIG. 3. The oxidation states of Si atoms averaged for a given distance along [001] direction for the whole supercell under different n .

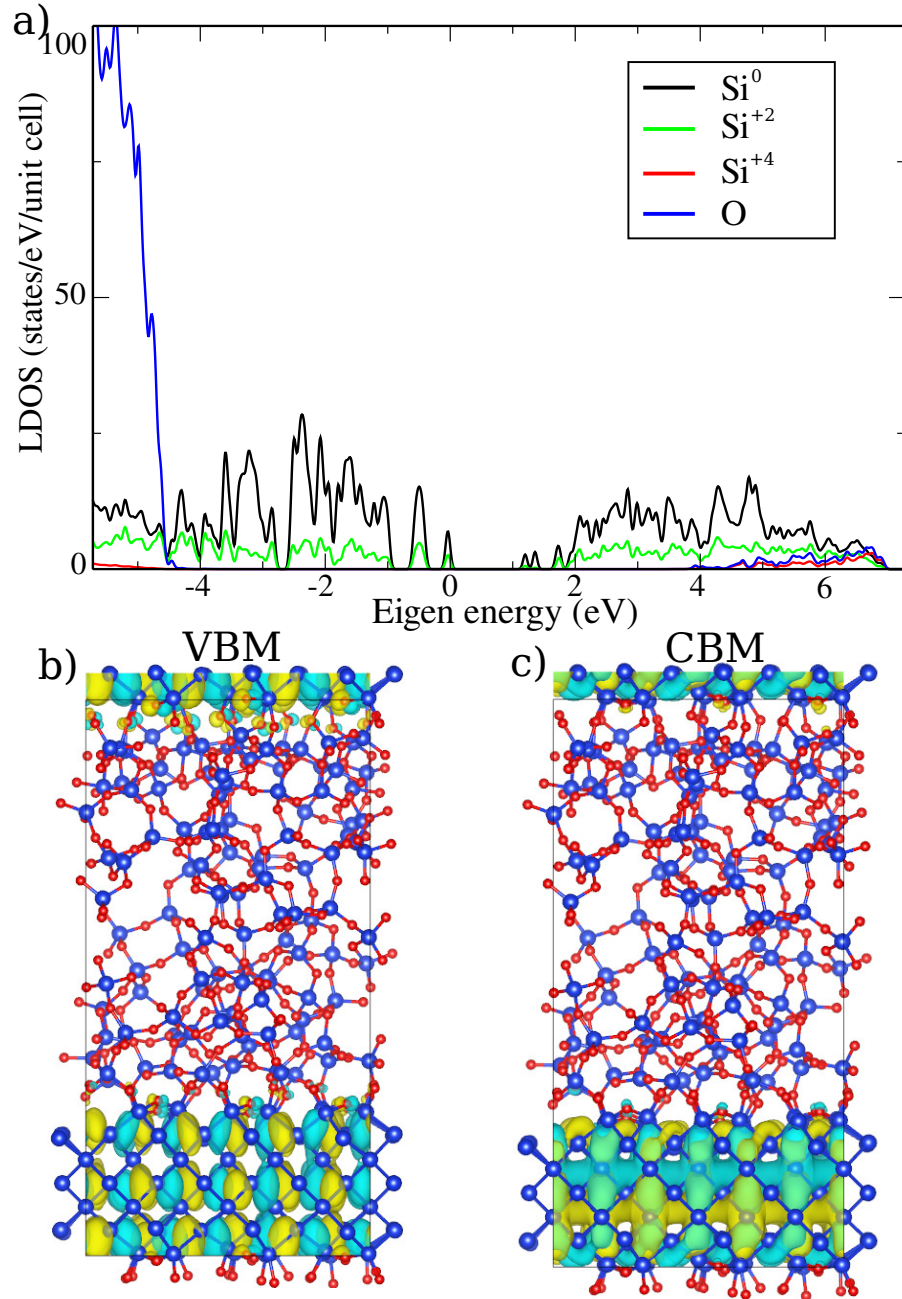


FIG. 4. a) The HSE calculated local density of states for Si⁰ atoms (Si-bulk part), Si⁺² (transition region), Si⁺⁴ (SiO₂-bulk part) and O (SiO₂-bulk part) atoms obtained from the $n=2$ structure. Here, the Si⁺⁴ and O atoms are from the middle of the SiO₂-bulk part to exclude the contribution from interfacial region. 0 energy is set to be at the valence band minimum. Real space wavefunction isosurface for the b) valence band maximum (VBM), and c) conduction band minimum (CBM) of this structure.

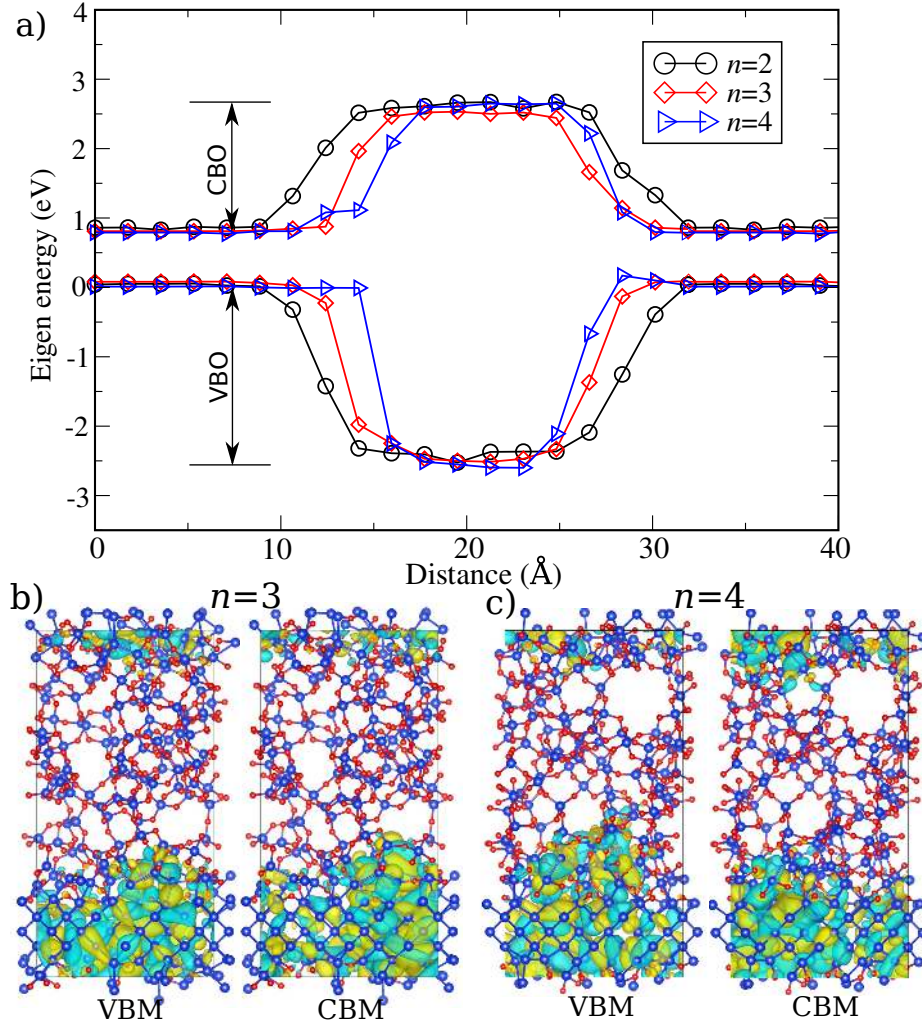


FIG. 5. a) The GGA calculated VBM and CBM averaged for a given distance along [001] direction across the interface for structures with $n=2, 3$ and 4 . Left and right ends correspond to the Si-bulk part, with 0.8 eV band gap; the middle part corresponds to the SiO₂-bulk part, with around 5.2 eV band gap. The valence band offset is computed as 2.5 eV, and the conduction is 1.8 eV. b) The VBM and CBM wavefunctions in real space for the structures with $n=3$ and 4 .

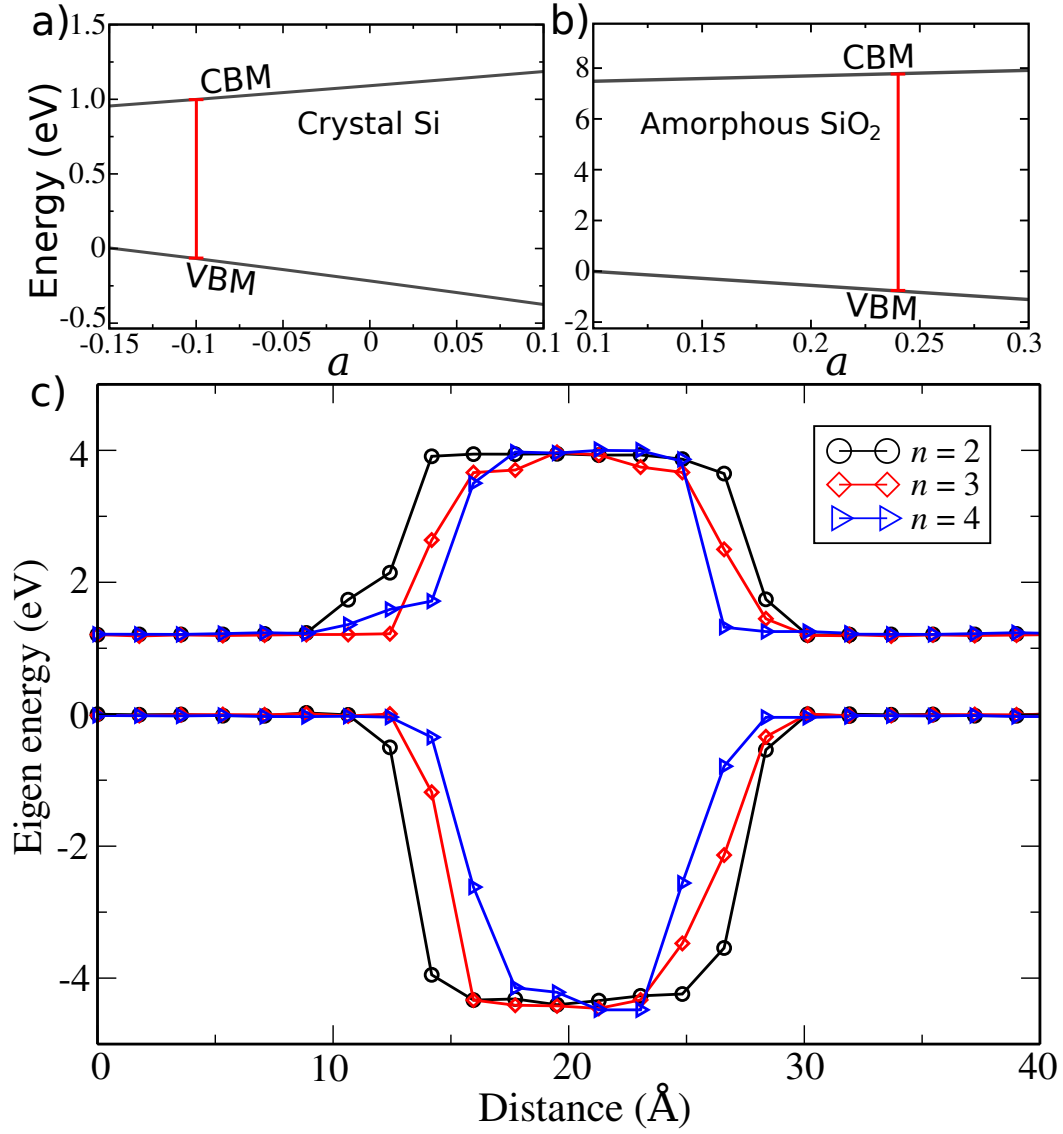


FIG. 6. a) CBM and VBM energy of silicon crystal calculated by different mixing parameter α of HSE. Here, α is adjusted by a as described in Methods. b) VBM and VBM energy of the 243-atom amorphous SiO₂ with different α . c) HSE calculated band offset of the structure for the structures with $n=2, 3$ and 4.